RELATIVE TIMING AND SPECTRA OF SOLAR FLARE HARD X-RAY SOURCES

SÄM KRUCKER [1] and R. P. LIN[1,2]

[1] *Space Sciences Lab, University of California, Berkeley, CA 94720-7450, U.S.A.*
[2] *Physics Department, University of California, Berkeley, CA 94720-7450, U.S.A.*

Abstract. Hard X-ray lightcurves, spectrograms, images, and spectra of three medium-sized flares observed by the Reuven Ramaty High-Energy Solar Spectroscopic Imager (RHESSI) are presented. Imaging spectroscopy of the 20 February 2002, 11:06 UT flare at $10''$ spatial resolution, comparable to the best previous hard X-ray imaging from *Yohkoh*, shows two footpoints with an ~ 8 s delay of peak emission between footpoints. Subsequent imaging at $\leq 4''$ shows three sources consistent with two separate loops and simultaneous brightening in connected footpoints. Imaging for the simple two footpoint flare of 2 June 2002 also shows simultaneous footpoint brightening. The more complex 17 March 2002 flare shows at least four different sources during the main peak of the event, and it is difficult to clearly demonstrate simultaneous brightening of connected footpoints. Non-thermal power laws are observed down to $\sim 12–13$ keV without flattening in all these events, indicating the energy content in energetic electrons may be significantly greater than previously estimated from assumed 25 keV low energy cutoff. Simultaneously brightening footpoints show similar spectra, at least in the three flares investigated. Double-power-law spectra with a relatively sharp break are often observed.

1. Introduction

During the flare impulsive phase, a double footpoint structure is often observed with the two footpoints brightening simultaneously to within a fraction of a second (Sakao *et al.*, 1994, 1996). These coincide, spatially and temporally, with Hα and white-light brightenings. For some flares occurring near the solar limb, the *Yohkoh* Hard X-ray Telescope (HXT) has detected a co-temporal, weaker, hard X-ray source in the corona (Masuda *et al.*, 1994; Alexander and Metcalf, 1997) above the soft X-ray loop linking the hard X-ray footpoints. This source has been interpreted as evidence for energy release by magnetic reconnection in a region above the soft X-ray loop.

Very rapid transport of energy from the release site down to the footpoint interaction regions is required. This can only be achieved by fast electrons streaming down the loop and depositing their energy in lower coronal and chromospheric footpoints, implying that nonthermal, tens-of-keV electrons are interacting with a cool ($T < 10^5$ K) environment. The resulting heating of the ambient gas leads to evaporation of chromospheric material and flare radiation in the visible, UV/EUV and soft X-rays. Hard X-ray studies of electron time-of-flight (Aschwanden *et al.*,

1996) further support this nonthermal thick-target model. RHESSI's hard X-ray imaging, with much wider energy range (3 keV to 17 MeV), higher dynamic range, and finer spatial (2.3 arc sec) and spectral resolution (1 keV FWHM) than *Yohkoh* HXT, is designed to study these sources and electron streaming in detail. Here we present the first results for three flares, concentrating on the timing, imaging, and spectral signatures in hard X-rays to provide information on the acceleration and propagation of the energetic electrons in the flares.

2. Data Analysis

Overview plots (Figures 1, 6, 8) are used to select flare events for study. To produce these plots, the RHESSI counts are binned in energy in two ways: (1) The photons are binned into 4 energy bands to make time profiles at 1 second resolution (second panel from top); or (2) into 32 logarithmically spaced energy channels to make count spectrogram plots (third panel from top). The decrease in counts below ~ 10 keV in these plots is due primarily to absorption by the thin shutter (cf., Lin *et al.*, 2002) that is in front of the detectors during these observations. The logarithmic binning produces a clearer representation by flattening out the otherwise steep spectrum. Overview plots of this kind are available online at *http://sprg.ssl.berkeley.edu/~krucker/hessi_plots*.

2.1. Imaging

For all events, cleaned images (Hurford *et al.*, 2002) averaged over one rotation period (~ 4 s) are constructed every second around the time of the HXR peak. Hence, there is time overlap in these time series and short lived sources could be smeared out. The standard RHESSI software corrects these images for efficiency using the diagonal elements of the spectral response matrix only (cf., Hurford *et al.*, 2002). Generally, grid 2 and higher are used giving a resolution down to 4 arc sec. Including grid 1 (2.3 arc sec) did not enhance the image quality for these events at the present state of the calibration (Figure 2, bottom). These time series of images allowed the event evolution to be studied in detail, and the time profiles of individual sources to be derived. In particular, it allows the determination of when sources appear and disappear, and the selection of the time interval to integrate over to get the best possible image of a particular source.

2.2. Imaging spectroscopy

To determine the spectrum of an individual source, images at 20 logarithmically spaced energy bands are made. Individual sources are then selected and the flux within each source is summed separately at each energy. An error estimate is approximated from the residual map provided by the CLEAN algorithm. The maximum in the residual map outside the source is taken as a very rough approximation

of a 3σ error. The same error is used to determine the uncertainties of the time profiles mentioned above. In the graphical representation, the derived errors are divided by 3 to represent a 1σ error bar.

As a first attempt, a very simple fitting of the derived flux spectra is used that will be improved in future work. A power law or broken power law is first fitted to the spectra above ~ 15 keV. The cutoff energy of the power law is chosen normally between 10 to 15 keV; at lower energies the power law contribution is neglected. This power law fit is then subtracted from the observed spectrum before fitting a thermal spectrum to the values below ~ 10 keV. The thin shutter (cf., Lin *et al.*, 2002) was in front of the detectors for all the flares presented here. This shutter absorbed most of the photons below ~ 10 keV. Therefore, for the events presented here, fitting below 10 keV depends critically on the calibration.
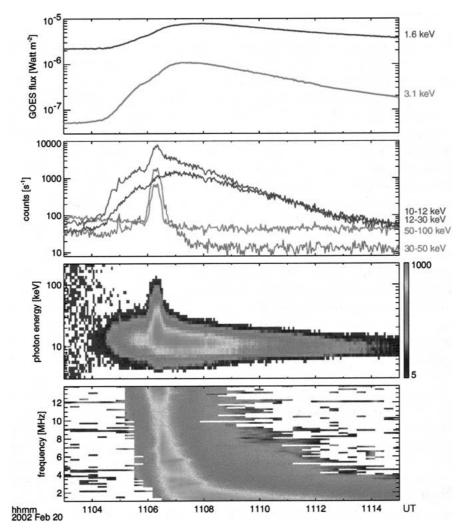
Fitting of the thermal component in the HXR footpoint spectra has an additional, more severe problem. It is very difficult to separate the thermal emission of the footpoint from the much brighter thermal emission of the loop often seen between the footpoints. Contamination from the thermal loop source (due to side-lobes) might contribute significantly to the flux in the selected source region of the HXR footpoints. Therefore the fitted thermal emission of footpoints presented in this work are preliminary and need more investigation. The derived values appear reasonable, between 10–20 MK; however, because of the above mentioned difficulties, the derived footpoint temperature and emission measure are not discussed in detail.

3. Observations

Three events are presented here: 20 February 2002, 11:05 UT; 2 June 2002, 11:44 UT; and 17 March 2002, 19:28 UT. All these events were selected because they show prominent hard X-ray peaks above 30 keV. The 20 February flare is presented in detail, the 2 June flare is selected as an example of a simple two footpoint source, and the 17 March flare is an example of a very complex flare.
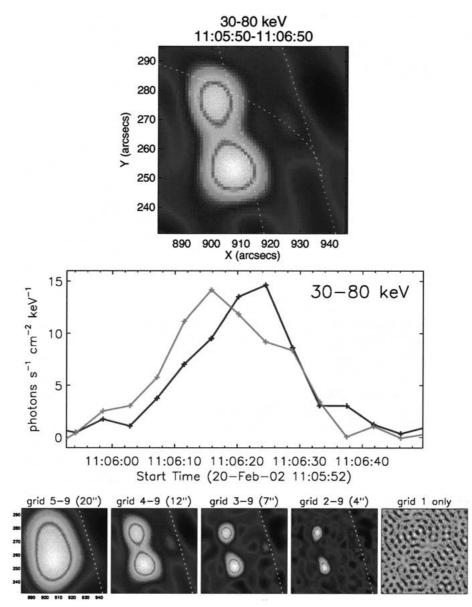
3.1. 20 February flare

The 20 February, 11:05 UT flare presented here is a smaller flare (GOES class C7.7) occurring on a day when 5 GOES M-class flares were observed. Nevertheless, this event was selected since only a single, simple HXR peak is seen. This event is also discussed by the images, by Aschwanden *et al.* (2002) studying the height at which the HXR emission originates, and by Sui *et al.* (2002) modeling the HXR emission. Additionally, this flare produced intense radio bursts that are compared with the HXR emission by Vilmer, Krucker, and Lin (2002).
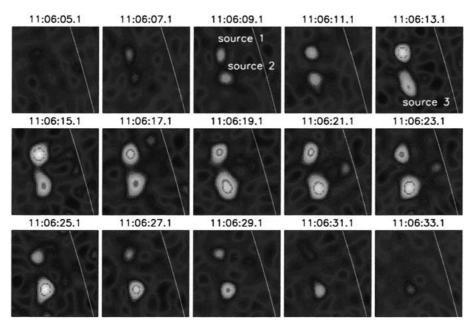
Figure 1. X-rays and radio waves overview plot of the 20 February 2002 flare. *Top*: GOES 1–8 Å (1.6 keV) and 0.5–4 Å (3.1 keV) lightcurves. *Second from top*: RHESSI lightcurves at four energies. *Third from top*: RHESSI spectrogram plot, the background has been subtracted. *Bottom*: WIND/WAVES RAD2 radio spectrogram. See the accompanying CD-ROM for color versions of this and other figures.

3.1.1. *Imaging*

Imaging around the hard X-ray peak reveals a flare location close to the west limb (N14 W79). At a spatial resolution of 10″, comparable to that of the *Yohkoh* HXT, two main HXR sources could be identified (Figure 2, top). Surprisingly, the maxima of the two sources did not occur simultaneously (Figure 2, bottom) contrary to the general behavior seen by Sakao *et al.* (1996). The southern source peaked about ∼ 8 seconds later than the northern source. However, imaging at resolution

Figure 2. Non-thermal X-ray image (30–80 keV) of the 20 February flare with a resolution of $12''$ (*top*). At this resolution, only two sources are seen that show different time profiles (in gray for the northern source) suggesting non-simultaneous brightening of footpoints (*middle*). Cleaned images with succesively better resolution are shown below. The last image is computed using the finest grid only (grid 1, $2.3''$) and does not show significant emission. All times in UT.
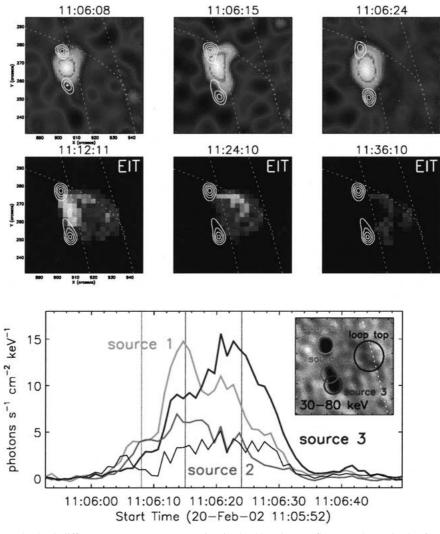
Figure 3. HXR images (30–80 keV, 7″ resolution) taken every 2 s with ∼ 4 s integration time of the 20 February flare are shown. The field of view is 64″ by 64″, the *white lines* give the location of the solar limb. All times in UT.
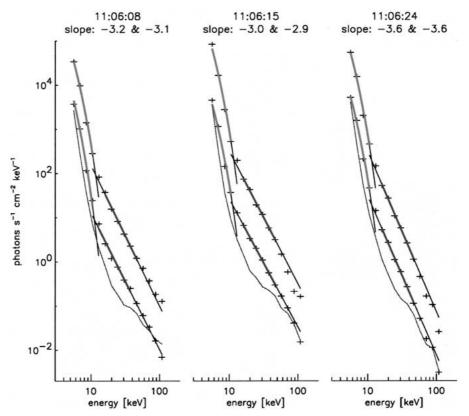
below 4″ and with a cadence of 1 second (with an integration time over ∼ 4 s, one spin period) showed three sources: Source 1 to the north, source 3 to the south, and a weaker, earlier peaking source 2 in-between but much closer to source 3 (Figure 3). With this third source, the observed temporal evolution could be made consistent with simultaneous brightening of connected footpoints in two loops; one loop connecting source 1 and 2, the second connecting source 1 and 3.

In the beginning of the HXR peak (around 11:06:08 UT), source 1 and 2 are seen brightening simultaneously, reaching only moderate fluxes. Then, source 3 appears when source 1 peaks, while source 2 is slowly disappearing. In a third and last phase, source 3 peaks with a weaker simultaneous brightening of source 1.

Figure 4 shows X-ray images of the three different phases. The thermal emission seen in the 6–9 keV images suggest a hot loop connecting source 1 and 2, but there seems to be no hot loop connection to source 3. However, loop connection to source 3 might be much fainter and therefore be lost in the residuals of the cleaned images. Difference images produced from EIT observations (Delaboudinière *et al.*, 1995) showing possibly the loop connecting source 1 and 2 some minutes later, but the uncertainty of the roll angle of EIT images, of the order of 10″ (private communication by Gallagher), makes it difficult to relate the HXR sources and the post flare loops seen in EIT.

Figure 4. The 3 different HXR sources appearing in the 20 February flare are shown in the *first row* of figures. The images show the thermal emission (6–9 keV) with the 30–80 keV HXR contours overlayed (levels are 30, 50, 70, 90%). Later in the event EIT 195 Å difference images show the post flare loops (*second row* of figures). To outline the position of the earlier occurring HXR sources, contours of the time averaged 30–80 keV emission are overplotted. The *bottom panel* shows the temporal evolution of the different sources, including a possible source above the EIT loop top (*black*). The circles in the insert mark the source locations, but do not represent the source sizes. The three *gray vertical lines* give the center time of the interval of the above shown images; time intervals are ~ 8 s, ~ 8 s, and ~ 16 s, respectively. All times in UT.

Figure 5. Spectra of the different sources outlined in Figure 4. Each plot contains two spectra, source 1 is always plotted on top and shifted by a decade, source 2 is only shown at the bottom of the first plot, source 3 in the remaining two spectra. Thermal fits are shown in *thick, medium gray* and power-law fits in *thick, dark gray*. The *gray lines* give rough estimates of the uncertainties. The *thick lines* give the range in energy used to make the fit, values above 50 keV are questionable.

Next to the three main sources, there may be a fourth source that might just be slightly above the EIT loop; this is discussed in Sui *et al.* (2002). The time variation of this possible loop top source is shown in Figure 4 (bottom) in black.

3.1.2. *Imaging Spectroscopy*
For the three different phases of the HXR peak, images reconstructed in 16 narrow energy ranges were used to provide energy spectra for the three sources seen (Figure 5). All spectra show power laws at high energies, extending down to ~ 12–13 keV. Since the thermal emission is of similar magnitude around 10 keV, only the energy range above ~ 15 keV is used for the power law fit. At energies above ~ 50 keV, the uncertainties are large and these points are not used in the fit. No break in spectra is seen in this energy range: This is not incompatible with spatially integrated spectra that show a break at higher energies (between 45 to 60 keV).
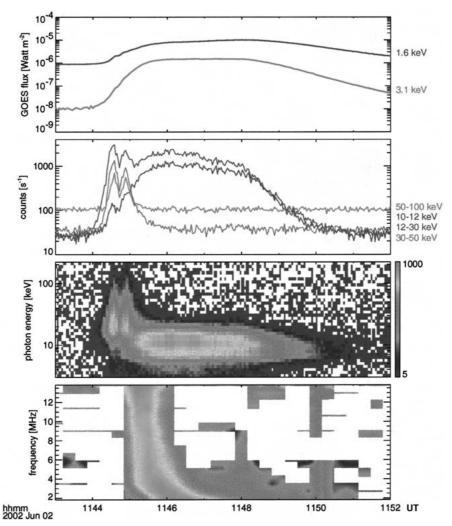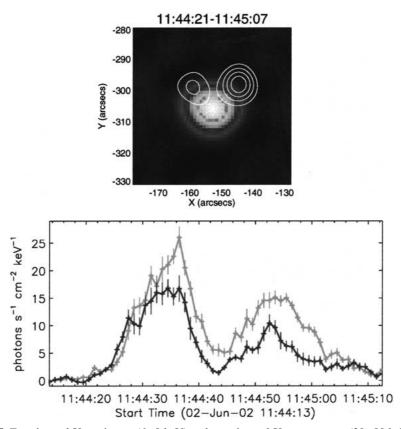
Figure 6. X-ray and radio wave overview plot of the event on 2 June 2002.

Spectra of loop-connected footpoints show very similar spectral slopes for all the three intervals. Power-law exponents between -2.9 to -3.2 are calculated for the first two phases, while the last peak gives a softer spectral exponent around -3.6. Spatially integrated spectra show power-law exponents between -3.1 to -3.4 for the first two phases, and around -3.6 for the last peak. Considering the early stage of data analysis, the agreement is good.

3.2. 2 JUNE FLARE

The 2 June, 11:44 UT flare (GOES class M1.0) occurred on a day with several low-M-class flares (Figure 6). It was selected for its impulsive onset with a rise
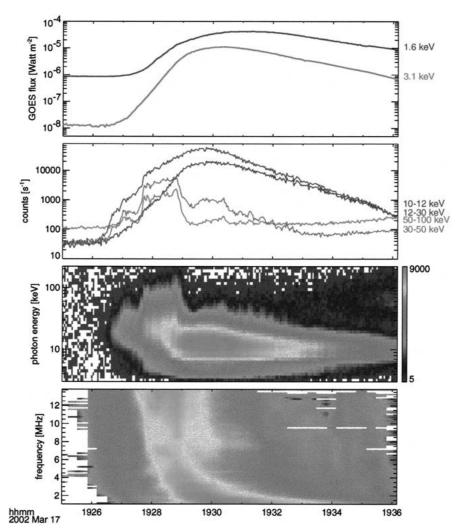
Figure 7. Top: thermal X-ray image (6–9 keV) and non-thermal X-ray contours (30–80 keV, levels are 30, 50, 70, 90%) averaged of the HXR peak of the 2 June flare are shown. *Bottom*: the time profile of the two sources are given. Times in UT.

phase of 3 min and its simple double-peaked HXR time profile. The images around the peak times show only two footpoints occurring near S19 E10 (Figure 7), and even after careful investigation, no other sources could be found. This simple flare geometry is a good test for simultaneity: first results (Figure 7, bottom) show that the two footpoints brighten simultaneously within the uncertainties.
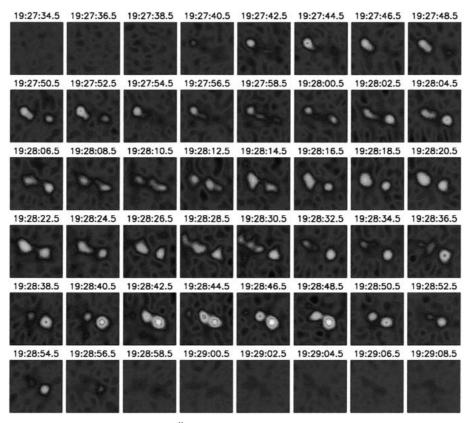
3.3. 17 MARCH FLARE

The GOES M4.4 flare occurring at S21 E17 on 17 March 2002 is an example of a more complex flare. The RHESSI data show three distinct groups of HXR peaks above 30 keV: rise (19:26:30–19:27:30 UT), main peak (19:27:30–19:29:00 UT), and decay (19:29:00–19:33:00 UT), which continues after the GOES flux is already decaying (Figure 8). The spatial distribution is also very complex with at least 4 different sources appearing during the main peak alone (Figure 9). With this complexity of the source structure, it is difficult for the source temporal evolution

Figure 8. X-ray and radio wave overview plot of the event on 17 March 2002. Note that the enhanced emission starting late in the event around ∼ 19:33 UT seen mostly above 30 keV is not of solar origin, but produced locally around the spacecraft by magnetospheric particles.

to be clearly interpreted as simultaneous brightening of loop-connected footpoints. Alexander and Metcalf (2002) analyze this event using the Pixon algorithm.

The main HXR peak (19:27:30–19:29:00 UT) was divided into two time intervals that were studied separately. The most prominent sources are two footpoints connected by a thermal loop seen between 19:28:38 and 19:28:50 UT (Figure 10, right). Earlier (19:27:36–19:28:36 UT), the source structure is more complex, showing an elongated source in the east (Figure 10, left) that most likely is composed of 3 sources (see time series of images shown in Figure 9). The source seen to the west seems to be the same source that later shows up during the main peak.
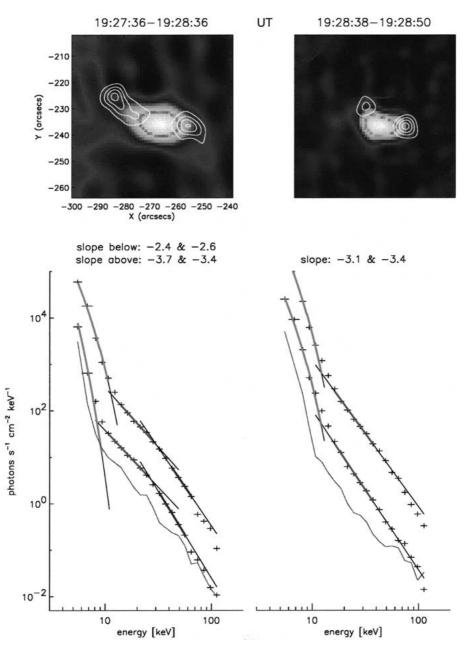
Figure 9. HXR images (30–80 keV, 7″ resolution) taken every 2 s with ∼ 4 s integration time of the 17 March event. Time in UT.

However, the second footpoint seen during the main peak is missing (or much fainter) during this earlier phase.

Interestingly, the fits to the spectrum of the sources seen in the earlier phase and the main peak give different results: the spectra in the earlier phase can only be fitted with a broken power law with a steeper spectra above ∼ 30 keV, whereas the main peak can be fitted with a single power law up to 60 keV. The similarity of the spectra for the two main sources in each time interval suggests a possible spatial (loop) connection.

4. Discussion

First results of HXR images and imaging spectroscopy obtained by the RHESSI mission reveal the great potential of this mission. Three medium-sized flares with rather short and impulsive onsets in X-rays are studied revealing the complexity of X-ray sources seen during a flare. Even if the HXR time profile shows only one,

Figure 10. Images and spectra of the inital HXR phase and the main HXR peak of the 17 March flare. The images show again the 6–9 keV thermal emission and the contours are the non-thermal 30–80 keV hard X-rays (levels are 30, 50, 70, 90%). *Below*, the spectra taken during these two time periods are shown. The spectrum of the western source is shown on top shifted up by a decade from the eastern source. The *shades* represent the same as in Figure 5 except that additionally a broken power law is fitted in *thick dark gray* to the earlier phase of the flare. Values above 65 keV are questionable.

simply shaped peak, several sources can be involved. Without adequate spatial resolution, these observations can be mistakenly interpreted as simple two-footpoint flares. By wrongly combining two or more sources into one source, the time history then shows non-simultaneous brightening of footpoints. Imaging with resolution down to 4″, however, reveals the complexity of source structure. The time evolution and the spectra of these sources are then found consistent with simultaneous brightening of connected footpoints. More detailed studies are need to give quantitative values and error estimates of the simultaneity. Thermal emission is observed to be coming from compact regions often connecting HXR footpoints.

Imaging spectroscopy with RHESSI gives for the first time the possibility to distinguish footpoints and other features in the images and to compute their spectra independently down to 3 keV with a spectral resolution of 1 keV. Generally, non-thermal power-law spectra are observed down to at least ~ 12 keV. This indicates that the lower energy cutoffs used in previous years of 20–25 keV (e.g., Crosby *et al.*, 1994) for the calculation of the total energy in energetic electrons are likely underestimating the energy content in non-thermal electrons by a factor of at least > 4 (assuming a power law index of 3). For microflares where the thermal component is weaker and at lower energies, making it easier to detect non-thermal emission below 10 keV, power laws extending even down to 7 keV are reported (Krucker *et al.*, 2002).

These first imaging spectroscopy results also show that simultaneously brightening footpoints have similar non-thermal power law indices, even if the absolute values of the spectra can be different. This similarity of the spectra provides independent support for the loop-connection of the two footpoints.

In the event of 17 March where statistics are most favorable, a break above 35 keV is observed in the spectra, with a steeper slope at higher energies. Later in the event during the main peak of the flare, the spectra, however, are best represented with a single power law fit. In events where the statistics are good, double-power-laws with a relatively sharp break appear to be common. Such spectra may have significant implications for the acceleration and/or energy loss processes.

References

Alexander, D. and Metcalf, T. R.: 1997, *Astrophys. J.* **489**, 442.
Alexander, D. and Metcalf, T. R.: 2002, *Solar Phys.*, this volume.

Aschwanden, M. J., Wills, M. J., Hudson, H. S., Kosugi, T., and Schwartz, R. A.: 1996, *Astrophys. J.* **468**, 398.

Aschwanden, M. J. *et al.*: 2002, *Solar Phys.*, this volume.

Crosby, N. B., Aschwanden, M. J., and Dennis, B. R.: 1993, *Solar Phys.* **143**, 275.

Delaboudinière J.-P. *et al.*: 1995, *Solar Phys.* **162**, 291.

Sui, L., Holman, G. D., Dennis, B. R., Krucker, S., Schwartz, R. A., and Tolbert, K.: 2002, *Solar Phys.*, this volume.

Hurford, G. J. *et al.*: 2002, *Solar Phys.*, this volume.

Lin, R. P. *et al.*: 2002, *Solar Phys.*, this volume.

Krucker, S., Christe, S., Lin, R. P., Hurford, G. J., and Schwartz, R. A.: 2002, *Solar Phys.*, this volume.

Masuda, S., Kosugi, T., Hara, H., Tsuneta, S., and Ogawara, Y.: 1994, *Nature* **371**, 495.

Sakao, T., Kosugi, T., Masuda, S., Yaji, K., Inda-Koide, M., and Makishima, K.: 1994, *Proceedings of Kofu Symposium*, Kofu, Japan, p. 169.

Sakao, T., Kosugi, T., Masuda, S., Yaji, K., Inda-Koide, M., and Makishima, K.: 1996, *Adv. Space Res.* **17**, 60.

Vilmer, N. *et al.*: 2002, *Solar Phys.*, this volume.